Structural Analysis of AgI and Au/AgI Nanocomposite Films by Powder X-ray Diffraction: Evidence for Preferential Orientation

Mahnaz El-Kouedi,[†] Colby A. Foss, Jr.,[‡] Sheri A. Bodolosky-Bettis, and Robert E. Bachman*[,§]

Department of Chemistry, Georgetown University, Washington, D.C. 20057

Received: March 25, 2002

Nanoparticle composite materials composed of AgI nanorods in porous alumina, and Au/AgI heterojunction nanorods, also in alumina, were synthesized via a template synthesis method and characterized using X-ray powder diffraction. The X-ray data suggest that electrodeposition of AgI nanoparticles at room temperature leads to a 50:50 mixture of the zinc blende (cubic) and wurtzite (hexagonal) morphs of AgI. Annealing the samples results in a conversion of cubic AgI to hexagonal AgI. Preliminary texture analysis of the samples suggests that the AgI nanorods are preferentially oriented within the pores of the host matrix such that the *c*-axis of the hexagonal phase is aligned with the pore axis, resulting in fiber formation. Annealing increases the degree of orientation substantially. Similar analysis of the Au/AgI heterojunction samples reveals that the presence of Au also increases the degree of alignment in as-deposited AgI. This work, which represents the first attempt to perform texture analysis on template-synthesized nanoparticle systems, demonstrates the usefulness of X-ray diffraction for the characterization of nanoparticles and nanorods.

Introduction

Much of the recent exploration in the field of nanotechnology has been driven by the desire to produce ever smaller electronic and optical devices.[1−3] Several research groups have explored new synthetic schemes for the preparation of complex nanoparticle systems.[4−7] In particular, metal−semiconductor heterojunctions have been recognized as being of significant technological importance as they are crucial to the construction of integrated circuits and other devices.[8,9] Given their importance and the drive to miniaturize electronics, it is not surprising that the synthesis and characterization of these types of heterojunctions in the nanoregime has begun to attract attention. A few examples of such structures have been reported in the literature recently, including cadmium chalcogenides on nickel substrates[10] and Cu−CuO nanoparticles.[11]

We recently reported the synthesis and optical characterization of Au/AgI heterojunctions embedded in an anodic alumina host matrix.[12,13] Embedding nanoparticles within such a dielectric host template improves the stability and handling of the material, and also allows for (a) the uniform alignment of nonspherical nanoparticles within the matrix, and (b) control of the proximity of two particles within a given pore.[14] Figure 1 is a schematic representation of our Au/AgI heterojunctions within a porous aluminum oxide host matrix illustrating the role of the host in orienting the particles. In this report we have turned our attention to the internal, i.e., crystalline, structure of these interesting nanostructures using powder X-ray diffraction (XRD). These studies have allowed us to examine issues such as the crystallinity and crystal structure of our nanoparticle composites, including preferential orientation of the crystallites within the pores. We have also explored the structural changes that occur upon annealing of the films. To our knowledge, detailed structural studies of multicomponent nanoparticles within a dielectric host media have not been previously reported.

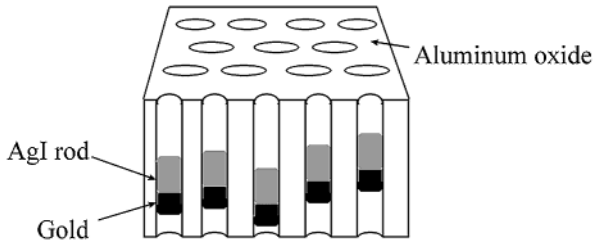

Figure 1. Schematic representation of Au/AgI heterojunction nanorods within a porous anodic alumina host matrix.

Experimental Procedures

General Considerations. The details of the preparation of nanoporous alumina films[15,16] and the AgI and Au/AgI composites[12] have been described elsewhere. For the present work, the alumina films were ca. 50 mm thick and the pore size was ca. 32 nm in diameter. Approximately 30−40 nm of silver metal was sputtered onto one face of the detached alumina film (barrier side) using an Anatech 10.2 plasma deposition device. This silver coating provided the electrical contact necessary for subsequent electrodeposition and oxidation steps. The total area of the porous alumina film subject to electrochemical modification was 3.14 cm^2. In the following discussion, all references to the number of coulombs (*C*) passed in a given synthesis step pertain to this total working electrode area. The pore area and volume fractions of the alumina films are ca. 0.3. An EG&G PARC Model 273 potentiostat equipped with a digital coulometer was used in all electrochemical procedures. All Ag depositions were done potentiostatically at an applied voltage of −0.6 V vs a silver−silver chloride reference (Ag/AgCl).

AgI Nanocomposite Films. After the sputtering step described above, a silver foundation of roughly 5.5 C was

* Corresponding author. E-mail: rbachman@sewanee.edu.
[†] Current address: Department of Chemistry, Pennsylvania State University, University Park, PA 16802.
[‡] Current address: Trex Enterprises Corporation, 3038 Aukele Street, Lihue, HI 96766.
[§] Current address: Department of Chemistry, 735 University Avenue, University of the South, Sewanee, TN 37383.

10.1021/jp020802b CCC: $22.00
Published on Web 06/29/2002

electrodeposited from a silver thiocyanate solution.[17] 1.5 C of this silver was then converted to silver iodide using a method adapted from Jaya et al.[18] A solution of 1M KI (prepared from Fisher ACS grade KI) was introduced into the cell, and the Ag was oxidized via a potentiostatic oxidation at 0.1 V vs Ag/AgCl. After the oxidation step, the entire alumina composite film was immersed in concentrated nitric acid to digest the unconverted Ag foundation. The film was washed with deionized water and allowed to air-dry overnight. The films are somewhat light-sensitive and were therefore stored in the dark.

Au/AgI Composite Films. After the sputtering step described above, a 4 C silver foundation was electrodeposited. The gold portion of the composite was then electrodeposited at −0.9 V vs Ag/AgCl from an Au(I) plating solution (Orotemp 24, Technic, Inc., Providence, RI). The amount of gold deposited corresponded to 0.5 C. A second 1.5 C layer of Ag was then electrodeposited on top of the gold. After this second layer of silver was deposited, the cell was thoroughly rinsed with deionized water to remove any free metal ions. The upper layer of silver was then converted to AgI using the method described above. Once this conversion was complete, nitric acid was again used to remove the silver foundation. After the films were washed with water, they were left to air dry overnight in the dark.

Sample Annealing. Each film sample was broken into two sections, the as-deposited film and the annealed film. The section to be annealed was placed in an oven at 60 °C and the temperature was raised to 120 °C at a rate of 1°/min. The temperature was held at 120 °C for 1 h and then decreased back to 60°, again at 1°/min.

Characterization. Optical and TEM characterization of such composites were performed previously.[12,13] The X-ray powder diffraction experiments were performed on a Rigaku *R*-Axis Rapid diffractometer equipped with an image plate detector. Graphite monochromated Cu Kα radiation ($\lambda = 1.54$ Å) was used throughout, with an instrument power of 2.12 kW (46 kV and 46 mA). A 300 micron collimator was used for all measurements. On the basis of a pore diameter of 30 nm, and a porosity of 30%, this implies that each measurement sampled approximately 3000 pores.

The sample films were mounted onto the goniometer head by taping a small portion of the composite films onto a steel needle. A CCD microscope camera was used to position the desired region of the sample in the X-ray beam and align it approximately perpendicular to the beam. All the measurements were carried out in transmission mode. The image plate images were converted to standard I vs 2q plots using the integration software included with the instrument and the following integration parameters: $10° < 2\theta < 140°$, $0° < \chi < 359.9°$, and an integration step of 0.01°. The data were analyzed with Jade 5 XRD Pattern Processing software. Peak positions and areas were determined by fitting diffraction profiles to Lorentzian, Voigt and pseudo-Voigt functions.

The pole figure data for texture analysis was acquired at $\omega = 11.85°$, $\chi = 55°$, and ϕ stepped through one complete revolution in 10° increments (36 images). The images were then converted to a standard pole figure using the routines incorporated into the Rigaku instrument control and data reduction software. In all samples examined in this way, texture analysis was performed for the reflection at 23.7 (2θ) only, which corresponds to the (002) hexagonal reflection and the (111) cubic reflection.

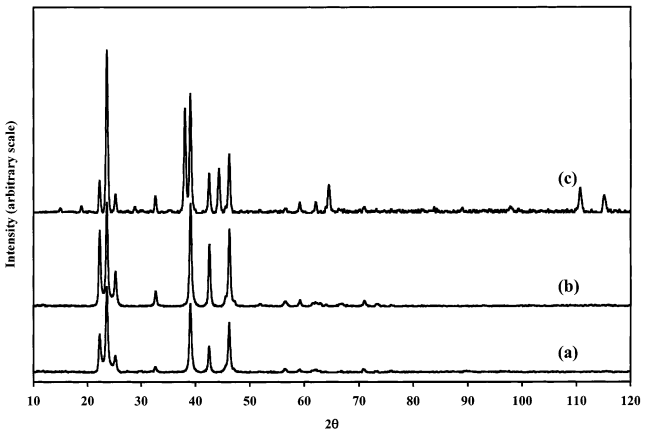

Figure 2. XRD patterns of the nanoparticle/alumina composites: (a) as-deposited AgI, (b) annealed AgI, and (c) as-deposited Au/AgI heterojunctions. The traces have been offset along the intensity axis for clarity.

Results and Discussion

X-ray diffraction experiments performed on the empty porous aluminum oxide matrix clearly show that it is amorphous. The only signal detected for these hosts is an extremely broad and diffuse background scatter, with no discernible diffraction peaks visible. This is in contrast to the results seen by Moskovits and co-workers in their study of CdSe nanowires in a similar matrix, in which they observed peaks assigned to the alumina host.[19] Given the details of the two experiments, it may be possible that this difference is a consequence of their leaving the oxide host attached to the aluminum plate on which it was grown. In any case, the amorphous nature of the host in our case creates an ideal situation for the study of the nanoparticle structure, as the host contributes only a weak background signal to the composites.

The diffractograms of as-deposited AgI show reasonably strong and sharp diffraction peaks out to 120° in 2θ, indicating a fairly high degree of sample crystallinity. After subtraction of the background signal (as determined by measurement of the empty host matrix), the diffraction pattern indicates the presence of a roughly 50:50 mixture of Wurtzite (hexagonal) and zinc blende (cubic) AgI (Figure 2a). No peaks due to other crystalline substances are observed. The phase assignment is based on the following factors. Three distinct diffraction peaks corresponding to the (100), (002), and (101) reflections of hexagonal AgI are clearly visible between 22° and 26° 2θ. However, the central (002) reflection is more intense than it should be in comparison to the outer two peaks. Since both of these phases can be conveniently thought of as a close-packed array of iodide anions with silver cations occupying half the tetrahedral holes, the (002) reflection of hexagonal AgI will be coincident with the (111) reflection of the cubic phase. Therefore, the "extra intensity" of this peak can be explained by the presence of the cubic phase. This assignment is also supported by the presence of the (220) reflection of the cubic phase at 39.1° 2θ.

This presence of a mixture of phases is in agreement with previous reports on nanoparticulate AgI grown in either a gelatin matrix or in an alumina host.[20] In the former case, Berry used the relationship shown in eq 1 to estimate the percentage of the cubic phase present in a sample of randomly oriented particles.[20a]

Using this

$$\%\text{cubic} = \frac{111_{\text{cubic}} + 002_{\text{hexagonal}}}{100_{\text{hexagonal}} + 101_{\text{hexangonal}}} \quad (1)$$

equation, we estimate that the as-deposited samples consist of between 50 and 60% cubic AgI. However, the presence of preferred orientation of the crystallites (vide infra) could also lead to an anomalously strong (002) reflection. Therefore, we used a similar analysis based on the ratio of the (100) reflection from the hexagonal phase to the (220) reflection from the cubic phase. This analysis, which also places the amount of cubic AgI between 40 and 55%, agrees reasonably well with the value obtained using Berry's method.

Diffractograms were collected at several random locations on a film in order to evaluate sample homogeneity. The resulting patterns were all qualitatively similar consisting of mixtures of both cubic and hexagonal phase. Additionally, films prepared in different deposition experiments showed little difference, including those films prepared at higher deposition potential. Consequently, it seems that the deposition process is relatively insensitive to the experimental conditions.

The as-deposited heterojunction Au/AgI composites display a diffraction pattern that is essentially the superposition of the pattern for Au and the pattern for AgI (Figure 2c). A small amount of AgSCN is also seen in these samples. While it is clear that this impurity arises from the silver deposition solution, the reason that it is seen in the heterojunction composites and not the pure AgI systems is not entirely clear. However, we have also found that when pure silver nanoparticles are electrochemically converted to AgBr, traces of AgSCN are detectable by XRD.[21] This result is in agreement with Pearson hard−soft acid−base theory[22] which predicts that the equilibrium for the displacement of thiocyanate by iodide is favorable but the displacement by bromide is not. This combination of results suggests that the AgSCN present in the heterojunction system is most likely the result of small inclusions of AgSCN made inaccessible to the solution phase by the gold nanoparticle. These inclusions are probably the result of incomplete removal of the AgSCN (the plating solution) between the deposition of the silver base and the gold nanoparticles.

As with the pure AgI samples, the AgI portion of these heterojunctions is a mixture of cubic and hexagonal phases. However, the hexagonal (002) reflection is clearly stronger than can be accounted for by considering the contribution of the cubic (111) reflection. Additionally, when the angle between the sample and the incident beam (ϕ) is larger than 30°, the appearance of the Debye ring corresponding to these reflections (i.e., the reflection at 23.7° 2θ) changes from a complete ring to a broken ring with a somewhat symmetric pattern (Figure 3). This change suggested to us the existence of a relatively high degree of preferred sample orientation.

Such preferential orientation of nanoparticles inside a host aluminum oxide matrix has been observed previously by Moskovits and co-workers and Yang et al. in their studies of cadmium sulfide nanowires.[19] In this system, which consisted of pure wurtzite (hexagonal) CdS, the XRD pattern suggested a preferential alignment of the crystallographic *c*-axis along the pore axis of the aluminum oxide host. They estimated the degree of alignment in these composites by measuring the relative intensity of the (002) reflection as compared to the (100) and (101) reflections. While such an analysis in our system would, in principle, provide a measure of the degree of orientation, the presence of cubic AgI complicates the problem, as it also results in an enhancement of the (002) reflection.

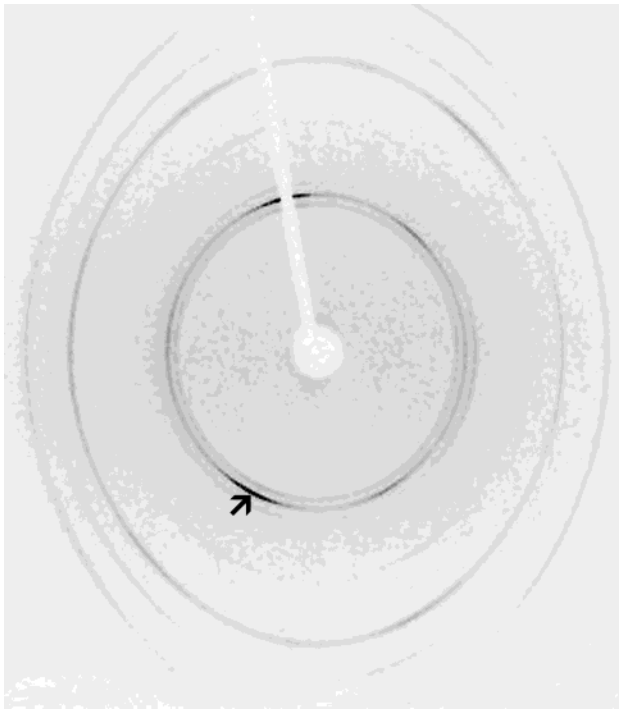

Figure 3. Picture of the Debye rings "captured" from image plate detector with the sample oriented at 30° relative to the incident beam ($\phi = 30°$) showing breaks in the ring at 23.7° (arrow), corresponding to the 002 hexagonal, 111 cubic reflections. This broken pattern is consistent with preferential orientation of the crystallites in the host alumina matrix.

Given the complications arising from the presence of both hexagonal and cubic AgI in these systems, we chose to investigate whether the cause of the anomalous intensity is preferred orientation by performing a preliminary pole figure, or texture, analysis of the sample, focusing on the 002 reflection (23.7° in 2θ).[23−26] These figures are stereographic representations of the diffraction intensity as a function of sample orientation and hence give detailed information about the orientation of the crystallites with respect to the host matrix. To our knowledge, such a texture analysis has never been performed on nanoparticle composites such as the ones reported here.

The pole figures for the as-deposited AgI and AgI/Au composites are shown in Figure 4. These pole figures show a maximum at a small angle (ca. 20°) from the normal direction (vertical) indicating some degree of alignment of the *c*-axis. The small deviation of this maximum from the normal direction is most likely an experimental artifact arising from difficulties ensuring a truly perpendicular initial alignment of the sample and the incident beam with the current experimental setup. Additional factors that may contribute to this effect are the fragile nature of the films and their tendency to warp slightly. Given these uncertainties, we will treat this maximum as if it corresponds to the normal direction in the remainder of the discussion.

In comparing the two pole figures in Figure 4, it is readily apparent that the overall degree of alignment is higher in the Au/AgI composite than in the AgI only sample. Furthermore, it is apparent that the secondary intensity maxima in both samples are not randomly distributed; rather, they occur at angles of approximately 30°, 70°, 90°, 110° and 150° relative to the normal direction maximum. The origin of the maxima at 30°, 90° and 150° are not clear to us; however, the maxima at 70° and 110° can be explained by considering the presence of cubic

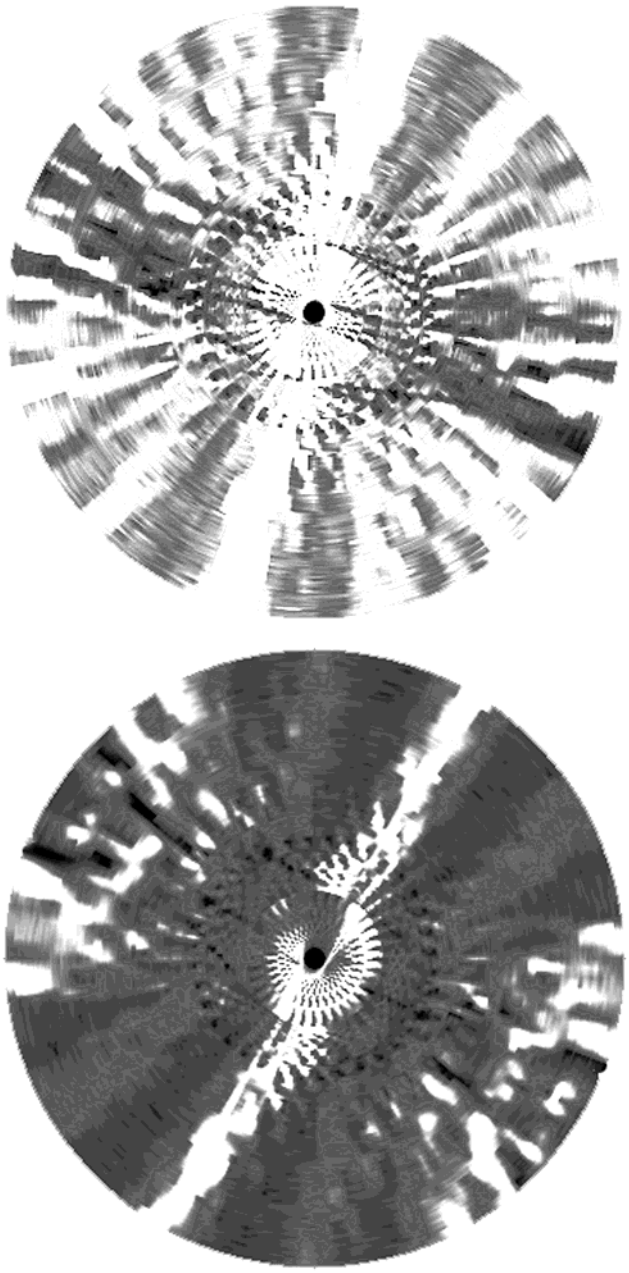

Figure 4. Pole figures for the 002 (hexagonal) reflection of the as-deposited AgI (top) and Au/AgI (bottom) nanoparticle films. Light regions represent high diffraction intensity.

AgI in the samples. Like the [002] direction of the hexagonal phase, the [111] direction (body diagonal) of the cubic phase corresponds to the close packing direction. Given the structural relationship between these two crystallographic directions in the two phases, it is reasonable to assume that the [111] direction of the cubic phase might also be aligned with the pore axis. If this is indeed the case, then the two maxima under consideration correspond to the [11−1] and [−1−11] directions, respectively. For reference, the calculated interzonal angles [111]:[11−1] and [111]:[−1−11] are 70.53° and 109.5°.

Moskovits and co-workers demonstrated that annealing their CdS samples led to an increase in the degree of alignment as measured by an increase in the (002) reflection intensity.[19] Consequently, we were interested in how thermal treatment would affect our samples, particularly the pure AgI system. As with the as-deposited samples, the presence of cubic AgI complicates the analysis.

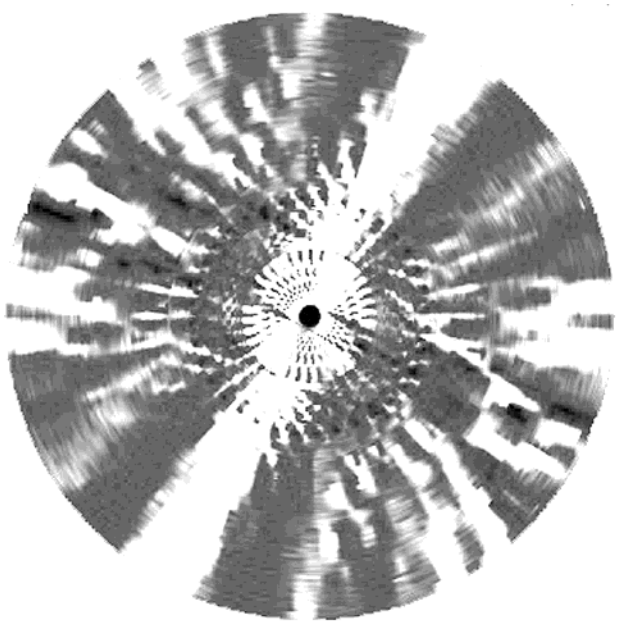

Figure 5. Pole figure for the 002 (hexagonal) reflection of the annealed AgI nanoparticle films. Light regions represent high diffraction intensity.

Since the cubic phase is less thermodynamically stable than the hexagonal, annealing should not only increase the degree of alignment but should also result in phase conversion from cubic to hexagonal. To estimate the amount of cubic phase present after the annealing process, we used methods identical to those used on the as-deposited samples (Figure 2b). Using Berry's method (eq 1) suggests that the amount of cubic phase present has been reduced to approximately 32%. Using the ratio of the (100) hexagonal phase to the (220) cubic phase results in an estimate of 25% cubic phase. Thus, as expected based on thermodynamic considerations, annealing significantly reduces the amount of cubic phase present.

The texture analysis of the annealed AgI samples provides an even more striking contrast (Figure 5). This figure shows intensity in essentially three directions: the normal as well as 70° and 110° from the normal direction. Hence, it appears that the annealing procedure has almost completely aligned the *c*-axis of the hexagonal phase and the [111] direction of the cubic phase with the pore axis.

Summary and Conclusions

The X-ray diffraction experiments reported here clearly demonstrate that our deposition procedure produces highly crystalline nanoparticles within a host matrix. As-deposited composites have some preferred orientation, which can be increased dramatically upon annealing. Annealing also results in a conversion of cubic AgI to hexagonal AgI. Preliminary texture analysis suggests that the *c*-axis of the hexagonal AgI and the [111] direction of cubic AgI both align with the pore axis. Additional studies are currently underway to address some of the outstanding questions raised by this study, such as how the presence of an Au substrate enhances the degree of orientation of the AgI layer, and if complete conversion from cubic to hexagonal AgI is possible.

Acknowledgment. CF acknowledges the National Science Foundation for support of this work (DMR 9625151). Funding for the X-ray diffractometer was provided by the National Science Foundation (CHE-0077637) and Georgetown University.

References and Notes

(1) Piner, R. D.; Zhu, J.; Xu, F.; Hung, S.; Mirkin, C. *Science* **1999**, *286*, 523.
(2) Huynh, U.; Peng, X.; Alivisatos, A. P. *Adv. Mater.* **1999**, *11*, 923.
(3) Jackman, R. J.; Brittain, S. T.; Whitesides, G. M. *J. Microelectromech. Syst.* **1998**, *7*, 261.
(4) Sandrock, M. L.; Pibel, C. D.; Geiger, F. M.; Foss, C. A., Jr. *J. Phys. Chem. B* **1999**, *103*, 2668.
(5) Huecko, A. *Appl. Phys. A.* **2000**, *70*, 365.
(6) Chen, W. C. W.; Nie, S. M. *Science* **1998**, *281*, 2016.
(7) Averitt, R. D.; Westcott, S. I.; Halas, N. J. *J. Opt. Soc. Am. B* **1999**, *16*, 1824.
(8) Rhoderick, E. H.; Williams, R. H. *Metal-Semiconductor Contacts*, 2nd ed.; Oxford University Press: Oxford, 1988.
(9) Aldao, C. M.; Weaver, J. H. In *Contacts to Semicondutors*; Brillson, L. J., Ed.; Noyes Publications: Park Ridge, 1993.
(10) Klein, J. D.; Herrick, R. D. II, Palmer, D.; Sailor, M. J.; Brumlik, C. J.; Martin, C. R. *Chem. Mater.* **1993**, *5*, 902.
(11) Switzer, J. A.; Hung, C. J.; Bohannon, E. W.; Shumsky, M. G.; Golden, T. D.; Van Aken, D. C. *Adv. Mater.* **1997**, *9*, 334.
(12) El-Kouedi, M.; Sandrock, M. L.; Seugling, C. J.; Foss, C. A., Jr. *Chem. Mater.* **1998**, *10*, 3287.
(13) El-Kouedi, M.; Foss, C. A., Jr. *J. Phys. Chem. B* **2000**, *104*, 4031.
(14) Beecroft, L. L.; Ober, C. K. *Chem. Mater.* **1997**, *9*, 1302.
(15) Diggle, J. W. In *Oxides and Oxide Films*; Diggle, J. W., Ed.; Marcel Dekker: New York, 1973; Vol. 2.
(16) Furneaux, R. C.; Rigby, W. R.; Davidson, A. P. *Nature*, **1989**, *337*, 147.
(17) Shumilova, N. A.; Zutaeva, G. V. In *Encyclopedia of Electrochemistry of Elements*; Bard, A. J., Ed.; Marcel Dekker: New York, 1978; Vol. 8, p 109.
(18) Jaya, S.; Rao, P. T.; Rao, P. G. *J. Appl. Electrochem.* **1988**, *18*, 459.
(19) (a) Routkevitch, D.; Bigioni, T.; Moskovits, M.; Xu, J. M. *J. Phys. Chem. B* **1996**, *100*, 14037. (b) Yang, J.; Zeng, J.-H.; Yu, S.-H.; Yang, L.; Zhou, G.; Qian, Y.-T. *Chem. Mater.* **2000**, *12*, 3259.
(20) (a) Berry, C. R. *Phys. Rev.* **1967**, *161*, 848. (b) Wang, Y.; Mo, J.; Cai, W.; Yao, L.; Zhang, L. *J. Mater. Res.* **2001**, *16*, 990.
(21) El-Kouedi, M. Ph.D. Dissertation, Georgetown University, Washington, DC, 2001.
(22) Miessler, G. L.; Tarr, D. A. *Inorganic Chemistry*, 2nd ed.; Prentice Hall: Upper Saddle River, 2000; pp 171−176.
(23) Bunge, H.-J. *Texture Analysis in Materials Science*; Butterworth & Co: London, 1982.
(24) Gilbert, M.; Ross, D. H.; Bowen, A. *Polymer* **1999**, *40*, 1233.
(25) Wessels, T.; Baerlocher, C.; McCusker, L. B. *Science* **1999**, *284*, 477.
(26) Lu, J.; Sue, H.-J. *Macromolecules* **2001**, *34*, 2015.